Iranian Journal of Chemical Engineering
Vol. 2, No. 2, 2005, IAChE

Numerical Simulation of the Hydrodynamics of a Two-Dimensional Gas–Solid Fluidized Bed by New Finite Volume Based Finite Element Method

M. H. N. Famili and M. K. Moraveji *
Department of Chemical Engineering, Tarbiat Modarres University P.O.BOX 14155-4838, Tehran, I.R. Iran.

Abstract
In this work, computational fluid dynamics of the flow behavior in a cold flow of fluidized bed is studied. An improved finite volume based finite element method has been introduced to solve the two-phase gas/solid flow hydrodynamic equations. This method uses a collocated grid, where all variables are located at the nodal points. The fluid dynamic model for gas/solid two-phase flow is based on the two-fluid model where both phases are continues and fully interpenetrating. For the gas and solid phases the Navier-Stokes equation based on the concept of local average is obtained. Results are verified against experimental data reported in the literature.

Keywords: Fluidized bed, control volume, finite element, gas solid, two-phase flow

Introduction

The subject of gas/solid flows has been studied quite extensively for several decades, mainly because of its important applications in chemical and petroleum industries such as pneumatic transport, catalytic cracking, and coal combustors. Gas/Solid flow systems are an essential part of many chemical processes and an understanding of the behavior of such flow systems can significantly enhance the design of such processes.

A gas fluidized bed is observed when a gas continuously flows through a bed of particles at an appropriate flow rate. The particles which are initially at rest, driven by the fluid drag force and the inter-particle forces from neighboring particles, start to move and exhibit complex and intriguing flow patterns, which in turn greatly affect the flow of the fluidized gas [1]. Gas/solid fluidized bed hydrodynamic behavior is complex and not yet fully understood. Especially the scale-up from laboratory to industrial scale is a problem. Equations describing the bubble behavior in gas/solid fluidized beds are (semi) empirical and often determined under laboratory conditions. For that reason there is no unique theory describing the behavior of bubbles in fluidized beds.

In the so-called "two fluid model'' both phases are considered to be continuous and fully interpenetrating. Both phases are described in terms of separate conservation equations with appropriate interaction terms representing the coupling between the phases. All the particles are assumed to be

* - To whom correspondence should be addressed, Email Address: m-moraveji@araku.ac.ir

identical, characterized by a density, form factor and a coefficient of restitution. The motion of a system of solid particles suspended in a Newtonian fluid can be completely described by the Navier-Stokes equations. Specification of the proper initial and boundary conditions would enable the determination of the hydrodynamics of the fluidized beds.

In recent years computational fluid dynamics (CFD) in multiphase flow has become a well accepted and useful tool in modeling gas/ solid flow systems and much progress has been made in developing computer codes for describing the fluidized beds. Although the tools for applying *single-phase* flows in CFD are widely available, application of *multiphase* CFD is however still complicated from both the physical and the numerical point of view. Moreover, the research efforts of most groups in this field are aimed at the development of still more detailed CFD models for the two-phase flow. Most of the developed models are based on a two - phase flow description - one gas and one solid phase. In the discrete solution of the convection and the diffusion problems, control volume based finite element methods are popular. One reason for this is that the methods combine the intrinsic geometric flexibility of finite element methods with the desirable, direct physical invocation of a conservation principle to clearly identify and delineate the control volume comprising the domain.

Here we have developed a new formulation of the control volume based finite element (CVBFE) method that has used the momentum equation implicitly. In this study, improved CVBFE has been applied to study the bed hydrodynamic behavior in a two-dimensional Cartesian cold flow in the riser section of a fluidized bed reactor.

Gas-Solid Two Phase Flow Model

The first step in the fundamental understanding of fluidization is usually attributed to Davidson [2] for his analysis of a single bubble motion in an infinite fluid bed. The Davidson model has been further developed by others.

Since there are a variety of such models it is convenient to catalog them as classical models [2, 3, and 4], dimensional analysis (scaling) [5, 6, 7] and hydrodynamic models [8, 9, 10]. Dimensional models were used to correlate and scale hydrodynamic phenomena in fluidization. Hydrodynamic models are used to predict the hydrodynamics of the fluidized bed. Numerical schemes based on mathematical models of separated particulate multiphase flow have used the continuum approach for all the phases or a continuum approach for the fluid phase and a lagrangian approach for the particle.

Continuum-continuum (or Eulerian-Eulerian) approach considers the particulate phase to be a continuous fluid interpenetrating and interacting with the fluid phase [11].

From a macroscopic viewpoint the solid phase in a gas-solid fluidization system behaves like a kind of fluid, thus most numerical simulations of fluidized beds assume that the solid phase is a continuum. For this reason, most models reported in the literature are based on a two-fluid model (TFM). In the TFM, both phases are considered to be continuous and fully interpenetrating. Anderson and Jackson [12] and Pritchett [13] first proposed the TFM. The proposed models have zero gas and solid viscosities. These models successfully predict physical behavior dominated by the drag between the solid phase and the gas phase, like the formation of bubbles at a single orifice. Gidaspow [10] reviewed three hydrodynamic models of fluidization and has shown that these models, with zero gas and solid viscosity, were able to predict a great deal of the behavior of bubbling beds, because the dominant mechanism of energy dissipation is the drag between the particles and the fluid. To overcome the deficiency of these inviscid models, for instance, predictiton of the force on tubes, a solid viscosity was added to the model [14]. The derivation of the continuum equations is usually based on the scale of particle size that were

replaced by local averaged variable which describe the macroscopic system of interest [15, 16].

There is extensive literature dealing with the derivation of continuum equations for multiphase systems and a number of con-tinuum models have been proposed [12, 13]. Pritchett [13], using an implicit finite difference procedure, was the first to obtain the numerical solutions of the full nonlinear continuum equations. Gidaspow [10] pro-posed a numerical model of a fluidized bed in which a numerical solution to the con-tinuum equations was developed for the analysis of bed hydrodynamics. Both phases were described in terms of separated con-version equations (Navier-Stokes type) with ap-propriate interaction terms represent-ting the coupling between the two phases. Viscous interaction forces for both phases were neglected in their code. Kuippers [15] proposed an improvement to the above models. This model differs from the previous work, in the incorporation of a Newtonian rheological model in the gas and solid phases and arrives at an excellent agreement with direct experimental results.

Governing Equations

In the TFM two sets of conservations are formulated, governing the balance of mass, momentum and thermal energy in each phase. Since the averaged fields of one phase are dependent on the other phase, interaction terms appear in the balance equations. These terms represent the momentum and energy transfer between the phases. For cold flow the thermal energy equation is neglected and thus we have:

Continuity Equation

Gas-phase continuity:

$$\frac{\partial(\varepsilon\rho_g)}{\partial t} + \nabla.(\varepsilon\rho_g \mathbf{u}) = 0 \tag{1}$$

Solid-phase continuity:

$$\frac{\partial[(1-\varepsilon)\rho_s]}{\partial t} + \nabla.[(1-\varepsilon)\rho_s \mathbf{v}] = 0 \tag{2}$$

Gas-phase momentum:

$$\frac{\partial(\varepsilon\rho_g \mathbf{u})}{\partial t} + \nabla.(\varepsilon\rho_g \mathbf{uu}) = -\varepsilon\nabla p - \beta(\mathbf{u}-\mathbf{v}) - \nabla.(\varepsilon\tau_g) + \varepsilon\rho_g \mathbf{g} \tag{3}$$

Solid-phase momentum:

$$\frac{\partial[(1-\varepsilon)\rho_s \mathbf{v}]}{\partial t} + \nabla.[(1-\varepsilon)\rho_s \mathbf{vv}] = -(1-\varepsilon)\nabla p + \beta(\mathbf{u}-\mathbf{v}) - \nabla.[(1-\varepsilon)\tau_s] - \nabla p_s + (1-\varepsilon)\rho_s \mathbf{g} \tag{4}$$

Where ε is the volume fraction of each phase, **u, v** are fluid phase and solid phase velocity vectors respectively, ρ is the density, τ is the viscous stress tensor, **g** is the gravity acceleration, p is the pressure, β is the interphase momentum transfer coefficient, P_s is the solids pressure. The conservation equations in a two dimensional rectangular coordinate for the transport of a property ϕ can be written in a general form [17]:

$$\left[\frac{\partial(\rho_i \varepsilon_i \phi)}{\partial t} + \nabla.(\rho_i \varepsilon_i \mathbf{V}_i \phi) - \nabla.(\varepsilon_i \Gamma_\phi \nabla\phi) = S_\phi\right] \tag{5}$$

Constitutive Equations

In order to solve the gas-solid conservation, the constitutive equations for gas/solid density, interphase momentum transfer coefficient, viscous stress tensor are required. The gas flow is cold and the fluid density ρ_g is related to the pressure by the ideal gas law. The other properties of the gas phase and the particle density ρ_s are set as a constant value.

For $\varepsilon \le 0.8$ the gas-solid interphase momen-tum transport coefficient is based on the well-known Ergun equation:

$$\beta = 150\,\frac{(1-\varepsilon)^2}{\varepsilon}\,\frac{\mu_g}{(\phi_s dp)^2} + 1.75(1-\varepsilon)\frac{\rho_g}{(\phi_s dp)}|u-v| \tag{6}$$

For $\varepsilon > 0.8$, the gas-solid interphase momentum transfer coefficient is based on the single sphere expressions derived by Wen and Yu [18]:

$$\beta = \frac{3}{4}Cd\;\frac{\varepsilon(1-\varepsilon)}{(\phi_s dp)}\rho_g|\mathbf{u}-\mathbf{v}|f(\varepsilon) \tag{7}$$

$$f(\varepsilon) = \varepsilon^{-2.65} \tag{8}$$

Here Cd is the drag coefficient; dp is particle diameter and ϕ_s is a measure of the sphericity. The relation given in Eq. (8) acts as a correction to the Stokes law for the free fall of a single particle and is introduced to account for the presence of other particles in the fluid [19]. The drag coefficient Cd is related to the particle Reynolds number:

$$Cd = \begin{cases} \dfrac{24}{\mathrm{Re}_p}\left[1 + 0.15(\mathrm{Re}_p)^{0.687}\right] & \mathrm{Re}_p \le 1000 \\ 0.44 & \mathrm{Re}_p > 1000 \end{cases} \tag{9}$$

$$\mathbf{Re}_p = \frac{\varepsilon\rho_g|u-v|dp}{\mu_g} \tag{10}$$

The fluid and solid viscous stress tensors are given by an expression analogous to the Newtonian fluid [12]. That is

$$\begin{aligned} \tau_g &= -\left\{\left(\lambda_g - \frac{2}{3}\mu_g\right)(\nabla.\mathbf{u})E + \mu_g\left[(\nabla\mathbf{u}) + (\nabla\mathbf{u})^T\right]\right\} \\ \tau_s &= -\left\{\left(\lambda_s - \frac{2}{3}\mu_s\right)(\nabla.\mathbf{v})E + \mu_s\left[(\nabla\mathbf{v}) + (\nabla\mathbf{v})^T\right]\right\} \end{aligned} \tag{11}$$

Where E is the Kronecker delta, λ_g and λ_s denote the bulk viscosities, μ_g and μ_s denote the shear viscosities of the gas and the solid phases respectively [20].

The solid phase pressure or particle-to-particle interaction force (∇P_s) is added to the momentum equation to make the system numerically stable [21] and, thus, to prevent the particle void fraction from reaching low values [10, 19].

P_s depends only on the porosity. The solid phase elastic modulus G (ε) defined by:

$$G(\varepsilon) = \frac{dp_s}{d\varepsilon} \tag{12}$$

By applying the chain rule the gradient of the solid phase pressure can be written as [15, 16]:

$$\nabla P_s = G(\varepsilon)\nabla \varepsilon \tag{13}$$

Gidaspow and Ettehadieh [19] and Ding [22] proposed an expression for the solid elastic modulus:

$$G(\varepsilon) = \frac{dP_s}{d\varepsilon} = 10^{8.76\varepsilon - 0.27}\ dyne/cm^2 \tag{14}$$

Numerical Method

The set of conservation equations, supplemented by the constitutive equations and the initial and boundary conditions, cannot be solved analytically and therefore a nume-rical method must be used. The numerical method used in the present investigation is an improved finite volume based finite element method [23]. This method uses a collocated grid, in which all variables are located at the nodal points. To prevent pressure checker-board, the objective of this method is to couple between velocity and pressure or porosity in the continuity equation. For this reason we use two types of velocity, convecting velocity and convected velocity (27). Rhie and Chow [24] were the first to use a collocated variable arrangement in the control volume based finite element method. Schneider and Raw [25, 26] introduced the concept of integration point equations in the incompressible flows to include the effects of the fluid flow physics on the integration point variable, thus improving the accuracy.

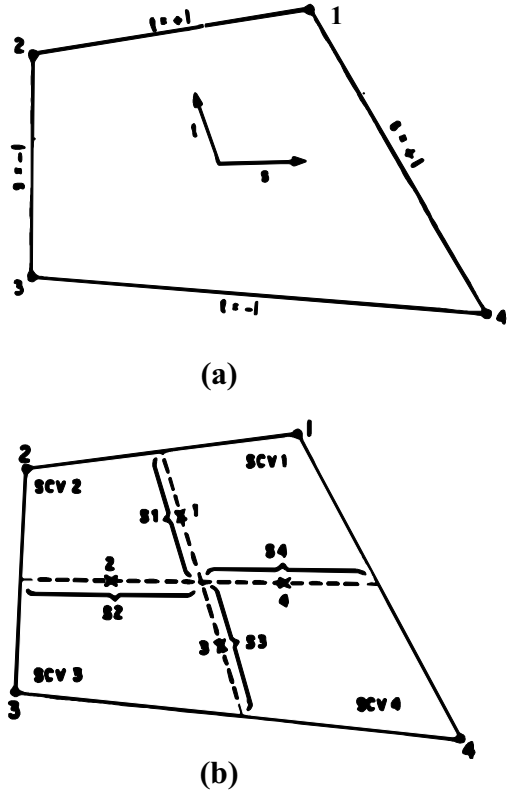

Figure 1. (a) typical element; (b) element with integration point, sub-control volumes and Subsurface labeled

Geometric Preliminaries

A typical element is shown in Figure 1a with a local non-orthogonal (s, t) coordinate system included. The sub-control-volume (SCV) boundaries are defined by the element external surfaces and lines corresponding to the local coordinate values of s=0 and of t=0. The four SCV surrounding the node then will form a control volume as shown in Figure 1b. The bilinear interpolation applied to describe the distribution of variables in the element is:

$$\phi = \sum_{i=1}^{4} N_i(s,t)\,\Phi_i \tag{15}$$

When derivatives are required, they can be evaluated according to

$$\frac{\partial \phi}{\partial x} = \sum_{i=1}^{4} \frac{\partial N_i(s,t)}{\partial x}\Phi_i \tag{16}$$

$$\frac{\partial \phi}{\partial y} = \sum_{i=1}^{4} \frac{\partial N_i(s,t)}{\partial y}\Phi_i \tag{17}$$

In the control volume based finite element method (CVBFE) for the conservation balance of a conserved quantity; we have to evaluate some surface and volume integrals on the control volume. For this, governing equations are discretized on an element by integration on the four SCV's and form the element matrix. Then discretized equation for each unknown on each node will form on element by element assembly process. For surface integration the argument of integral will be required at the midpoint of the SCV's line segments. These points will be denoted by integration points (ip).

Discretization

In an incompressible flow, density is independent of temperature and thus the continuity equation and momentum equations are decoupled from the energy equation, thus we can solve continuity and momentum equations individually.

In CVBFE method at first step we integrate governing equations on control volume. Applying the Gauss theorem we have

$$\frac{\partial}{\partial t}\iint_{scv_i}\rho\phi\ dv + \int_{ss_i}\rho u_j\phi\, ds_j - \int_{ss_i}\Gamma\frac{\partial\phi}{\partial x_j}ds_j - \iint_{scv_i}s_\phi = 0 \qquad j=1,2 \qquad (18)$$

For the transient term of the equation, a "lump mass approach" is employed. For constant ρ, a backward difference gives

$$\frac{\partial}{\partial t}\iint_{scv_i}\rho\phi\ dv \approx \left\{\frac{1}{\Delta t}\iint_{scv_i}\rho\,|J|dsdt\right\}\left[\phi_i^n - \phi_i^o\right] \qquad (19)$$

The diffusion term at the integration point is represented by

$$\int_{ss_1}\Gamma\frac{\partial\phi}{\partial x_j}ds_j \approx \Gamma_{ip1}\frac{\partial\phi}{\partial x}\Big|_{ip1}\Delta y_1 - \Gamma_{ip1}\frac{\partial\phi}{\partial y}\Big|_{ip1}\Delta x_1 \qquad (20)$$

in which the gradient components can be evaluated by using the usual bilinear shape function expressions.

For the discretization of the convection terms, convected and convecting velocity, must be evaluated in integration points. As the nature of the convection operator is parabolic we need to consider it in descretization to achieve stable and accurate results. The parabolic nature of convection terms does suggest that it is indeed highly desirable not only to upwind the convection operator, but also that this operator be skewed to reflect the local information propagation, this being along the local streamlines (25, 26).

A new method is presented to formulate the convecting and convected velocity. In this formulation we use streamline upwind and physical influence schemes and the transport equation to represent a new formula for the convected and convecting velocity.

Convected velocity

The convected velocity, which appears in the momentum equation to evaluate the surface integral of the momentum equation convection terms, must be integrated on the integration points

$$\rho \hat{u}_j \phi ds_i = \rho \hat{u} \phi ds_x \Big|_{ipi} + \rho \hat{v} \phi ds_y \Big|_{ipi} \tag{21}$$

Many approaches have been proposed for the evaluation of the convected velocity at the integration points. The problem that arises in conventional methods, is the failure to include the influence of the appropriate fluid flow or scalar transport physics on the integration point variables.

For the convection dominated problem as referred to above, the local upstream values will have a strong influence on the value of ϕ_{ip}, therefore the appropriate profile should have the form:

$$\phi_{ip} = \phi_{up} + \Delta \phi \tag{22}$$

where $\Delta\phi$ is a streamwise correction term (28, 29). With the central differencing scheme (CDS), second order accuracy for $\Delta\phi$ is obtained but it does not yield the physically correct influence and leads to "unphysical" oscillations especially in the high Peclet number. In the upwind or hybrid scheme, the physics of the problem are used for evaluation of the correction term. But these schemes input excessive false diffusion and consequently results are not accurate. The accuracy of the method is increased by improving the interpretation of the distribution of variables on the element compatible with the fluid flow. The best equation for this is the fluid flow governing equation. Schneider and Karimian [27] used the governing equation to obtain a relation that evaluates the convected velocity based on nodal variables.

In this regard, the conservative general form of the governing equation is written

$$\rho \frac{\partial \phi}{\partial t} + \rho \hat{u} \frac{\partial \phi}{\partial x} + \rho \hat{v} \frac{\partial \phi}{\partial y} = \Gamma \nabla^2 \phi + S_\phi + b \tag{23}$$

where, b is the gradient of the pressure.

In the stream wise direction, this equation will be

$$\rho \frac{\partial \phi}{\partial t} + \rho \overline{V} \frac{\partial \phi}{\partial s} = \Gamma \nabla^2 \phi + S_\phi + b \qquad \overline{V} = \left(u^2 + v^2\right)^{0.5} \tag{24}$$

s is the flow direction. After rearrangement of the above, the equation becomes

$$\frac{\partial \phi}{\partial s} = \frac{1}{\rho \overline{V}} \left[- \rho \frac{\partial \phi}{\partial t} + \Gamma \nabla^2 \phi + S_\phi + b \right] \tag{25}$$

In the streamline direction we discretize the Eq (14) as:

$$\phi_{ip} = \phi_{up} + \frac{\Delta s_{up}}{\rho \overline{V}} \left[- \rho \frac{\partial \phi}{\partial t} + \Gamma \nabla^2 \phi + s_\phi + b \right] \tag{26}$$

The second term represents streamwise correction. ϕ_{up} will be evaluated using the skewed streamline upwind method by accounting for the local flow direction.

Inside the bracket we have transient and diffusion terms that we must discrete. Discretizetion of the Laplacian term needs a second shape function; for this we used the bilinear shape function. For this problem, Karimian [27] considered the transient and diffusion terms explicitly by previous iteration or time steps. Schneider [28] considered only the transient term explicitly. In this scheme there are problems with the consistency and, at very little time steps, many oscillations are produced. The Karimian [27] method in transient and low Reynolds number has many shortcomings. For this reason we use the representation of Schneider [28] for discretizing the Laplacian operator as shown below

$$\left(\nabla^2 \phi\right)_{ipi} \approx \frac{\left(\sum_{j=1}^{4} N\big|_{ipi} \Phi_j\right) - \phi_{ipi}}{Ld^2} \tag{27}$$

Where Ld^2 is an appropriate diffusion length scale and for a rectangular element is given by

$$Ld^2 = \left(\frac{2}{\Delta x^2} + \frac{8}{3\Delta y^2}\right)^{-1} \tag{28}$$

With substitution of Eq. (16) in Eq. (15) and with backward discretization of transient term will have

$$\phi_{ipi} = \frac{\rho \overline{V}}{\lambda \Delta S_{up}} \phi_{up} + \frac{\sum_{j=1}^{4} N\big|_{ipi} \Phi j}{\lambda Ld^2} + \frac{\rho \phi^{o}_{ipi}}{\lambda \Delta t} + \frac{S_\phi}{\lambda} + \frac{b}{\lambda} \tag{29}$$

Where λ is defined as

$$\lambda = \frac{\rho \overline{V}}{\Delta S_{up}} + \frac{\rho}{\Delta t} + \frac{\Gamma}{Ld^2} \tag{30}$$

Therefore, all fluid flow physical affects convected velocity and as the relation is in implicit form, there is no need for extra memory storage. We repeat this procedure for two-phase flow and arrive at

$$\phi_{ipi} = \frac{\overline{\varepsilon \rho V}}{\lambda \Delta s_{up}} \phi_{up} + \frac{\sum_{j=1}^{4} N\big|_{ipi} \varepsilon_{ipi} \Phi_j}{\lambda Ld^2} + \frac{\rho \varepsilon_{ipi} \phi^{o}_{ipi}}{\lambda \Delta t} + \frac{S_\phi}{\lambda} + \frac{b}{\lambda} \tag{31}$$

$$\lambda = \frac{\overline{\rho \varepsilon V}}{\Delta S_{up}} + \frac{\rho \varepsilon_{ipi}}{\Delta t} + \frac{\varepsilon_{ipi} \Gamma}{Ld^2} + \rho \hat{u}_{ipi} \sum_{j=1}^{4} \frac{\partial N(ipi, j)}{\partial x} \varepsilon_j + \rho \hat{v}_{ipi} \sum_{j=1}^{4} \frac{\partial N(ipi, j)}{\partial y} \varepsilon_j \tag{32}$$

Convecting velocity modeling

The convecting velocity appears in the continuity equation and mass fluxes. The pressure checkerboard problem arises from the pressure field decoupling. The primary aim is to include

coupling between the pressure and the velocity in convecting velocity, because substitution of the convecting velocity in the continuity equation results in oscillation–free pressure and velocity. To prevent the pressure/velocity-decoupling problem, we use the momentum equation that includes the influence of pressure on the velocity. We rewrite the momentum equation in the streamline direction as:

$$\rho \frac{\partial u}{\partial t} + \rho \overline{V} \frac{\partial u}{\partial s} + \frac{\partial P}{\partial x} - \Gamma \nabla^2 u = 0 \tag{33}$$

After discretizing the convection term in the streamline direction, we will have

$$\rho \overline{V} \left(\frac{\hat{u}_{ip} - u_{up}}{\Delta s_{up}} \right) + \rho \frac{\partial u}{\partial t} + \frac{\partial P}{\partial x} - \Gamma \nabla^2 u_{ip} = 0 \tag{34}$$

By rearrangement of the Eq. (21), we will have

$$\hat{u}_{ip} = u_{up} + \frac{\Delta s_{up}}{\rho \overline{V}} \left(- \rho \frac{\partial u}{\partial t} + \Gamma \nabla^2 u_{ip} - \frac{\partial P}{\partial x} \right) \tag{35}$$

In Eq. (22) the effect of the pressure has appeared in the convecting velocity. In fact, inside the bracket of Eq. (22) is the momentum equation error (ε) and without the effect of the continuity equation. To include this effect we add the residual of the continuity equation to the bracket on the right-hand side of Eq. (22) (7, 8). The residual of the continuity equation is defined as

$$\dot{\varepsilon}_{ip} = \rho \left(\frac{\partial u}{\partial x} + \frac{\partial v}{\partial y} \right)_{ip} \tag{36}$$

If we rearrange the Eq. (23) in the fluid flow direction, we will have

$$u \dot{\varepsilon} = \rho \overline{V} \left(\frac{\partial u}{\partial s} \right)_{ip} - \rho \left(v \frac{\partial u}{\partial y} - u \frac{\partial v}{\partial y} \right)_{ip} \tag{37}$$

By substitution of Eq. (24) into Eq. (22), we will have

$$\hat{u} = \frac{\Delta s_{dn} u_{up} + \Delta s_{dn} u_{dn}}{\left(\Delta s_{up} + \Delta s_{dn} \right)} + \frac{\Delta s_{up}}{\rho \overline{V}} \left[- \rho \frac{\partial u}{\partial t} + \Gamma \nabla^2 u - \frac{\partial P}{\partial x} + \rho \left(u \frac{\partial v}{\partial y} - v \frac{\partial u}{\partial y} \right) \right] \tag{38}$$

In the above relation, the transient and diffusion terms are evaluated based on previous iteration data (8). To improve the above relation we use transient and diffusion terms implicitly. After using backward differencing method for the transient term and discretizing the Laplacian operator, we will have

$$\hat{u} = \frac{\rho \overline{V}}{\lambda \Delta s \Delta s_{up}} \left(\Delta s_{dn} u_{up} + \Delta s_{up} u_{dn} \right) + \frac{1}{\lambda} \left[\rho \frac{u^{o}}{\Delta t} + \frac{\lambda \sum_{i=1}^{4} N\big|_{ip} u_i}{Ld^{2}} - \frac{\partial P}{\partial x} + \rho \left(u \frac{\partial v}{\partial y} - v \frac{\partial u}{\partial y} \right) \right] \tag{39}$$

We repeat a similar procedure for $\hat{v}$. The advantage (40) of the above treatment is that all the variable employed are implicit and therefore we have highly accurate results for very low to very high ranges of Reynolds number and unsteady fluid flow. Again we repeat the above procedure for the two-phase flow and then we have:

$$\hat{u} = \frac{\overline{\rho \varepsilon V}}{\lambda \Delta s \Delta s_{up}} \left(\Delta s_{dn} u_{up} + \Delta s_{up} u_{dn} \right) + \frac{1}{\lambda} \left[\frac{\rho \varepsilon u^{o}}{\Delta t} + \frac{\sum_{j=1}^{4} N\big|_{ipi} \varepsilon_{ipi} u_j}{Ld^{2}} - \varepsilon \sum_{j=1}^{4} \frac{\partial N\big|_{ipi}}{\partial x} P_j + \rho \varepsilon \left(u \frac{\partial v}{\partial y} - v \frac{\partial u}{\partial y} \right) \right] \tag{40}$$

Simulation and Results of Gas/Solid Flow in a 2-D Riser

The new FVBFE method was used for the gas-solid two–dimensional flow in the riser section of the circulating fluidized bed (CFB). CFB are common in the petroleum industry. Figure 2 shows the riser section of a CFB used in the numerical simulation of gas/solid flow. The geometry of the riser is similar to the experimental set up used by Yang [29, 30]. Table (1) lists the experimental conditions of the test case. Initially the reactor is empty and the velocity of both gas and solid are set to zero. The simulated system was isothermal and the initial pressure was selected at atmospheric. Solid particles and gas were fed from the bottom of the riser uniformly. Gas and solid exited the system through the side outlet set below the closed up of the riser with a width of 0.14 m (similar to the side-inlets).

The inlet boundary conditions are completely specified for all dependent variables for both gas and particular phases of the prescribed flow. At the outlet, the normal gradient of the quantities is set to zero and exit pressure is specified. At the wall surface the normal gradient of all scalar variables and radial velocities of both phases are also set to zero. For the axial and tangential directions the gas velocity obeys the "no-slip" boundary condition. The particle phase velocity gradients at the riser is computed from the appropriate "wall function" [31], whereas the particulate phase is allowed to slip along the wall.

Table 1. Experimental Test Case Used for New Method [29, 30]

Particle diameter, d_p (m)	$5.4*10^{-5}$
Particle density, ρ_s (kg/m^3)	1545
Riser diameter(m)	0.14
Riser height(m)	11.0
Inlet gas axial velocity(m/s)	4.33
Particle mass flux(kg/m^2/s)	10.0
Inlet particle volume fraction	0.022

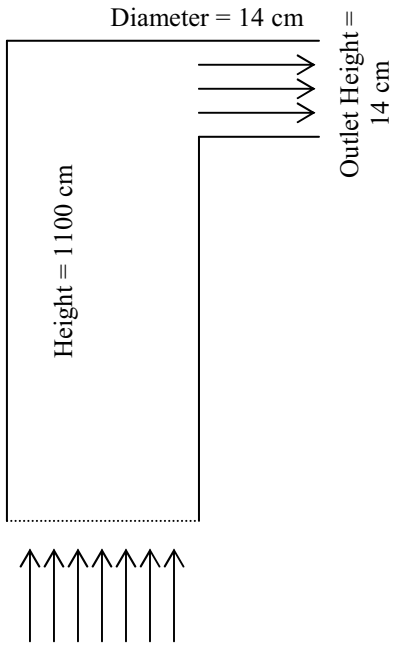

Figure 2. Geometry of the simulation system [29,30]

Figures (3, 4) show the comparison between the calculated radial gas and particle velocity distributions in the riser at heights of 1.6 and 6.6 m with experimental data [29,30] taken at the same heights. The particle velocity in the center of the riser was an upward, fast moving core surrounded by a slow moving layer near the wall. The agreement between the predicted and the measured velocities is remarkably good. Figure (5) shows the prediction of the velocity vectors of the gas/particle phases. Due to the very high solid (and gas) axial velocity at the center of the riser, the solid flux was at its maximum value, although the solid concentration was at its lowest value. Figure (6) shows the time-averaged axial particle volume fraction and pressure in the riser. The high-pressure drop at the bottom of the riser was due to the effect of particle feeding in that region. The pressure drop then decreased along the height of the riser resulting from decrease in the solid concentration. Due to the prediction of a bigger dilute core in the 2-D riser, lower flow resistance and a lower calculated pressure drop result.

Nomenclature

ds	Outward normal vector of area
e	Total energy per unit mass, J/kg
g	Gravity acceleration, ms^2
$\|J\|$	Jacobean determinant
P	Pressure, pa
q_i	Component of heat flux vector
s	Flow direction
S	Source term
$\hat{s},\hat{t}$	Local coordinate
t	Time, s
u	Velocity, cm/s
x, y	Global coordinate

Greek Symbols

β	Interphase momentum transfer coefficient
ε	Void fraction (volume fraction of particle)
ρ	Density, Kgm^{-3}
τ_{ij}	Stress tensor component
μ	Viscosity, gr/m.s
ϕ	Generalized conserved quantity
ϕ_s	spherity
Γ	General diffusion coefficient
∇	Divergence operator
∇^2	Laplacian operator

Subscripts

g	Gas phase
s	Solid phase
i, j, k = 1, 2	Einstein summation indices
ip	Integration point
up	Upstream
cv	Control volume

Superscripts

‾	Lagged value from the previous iteration
O	Previous time step value

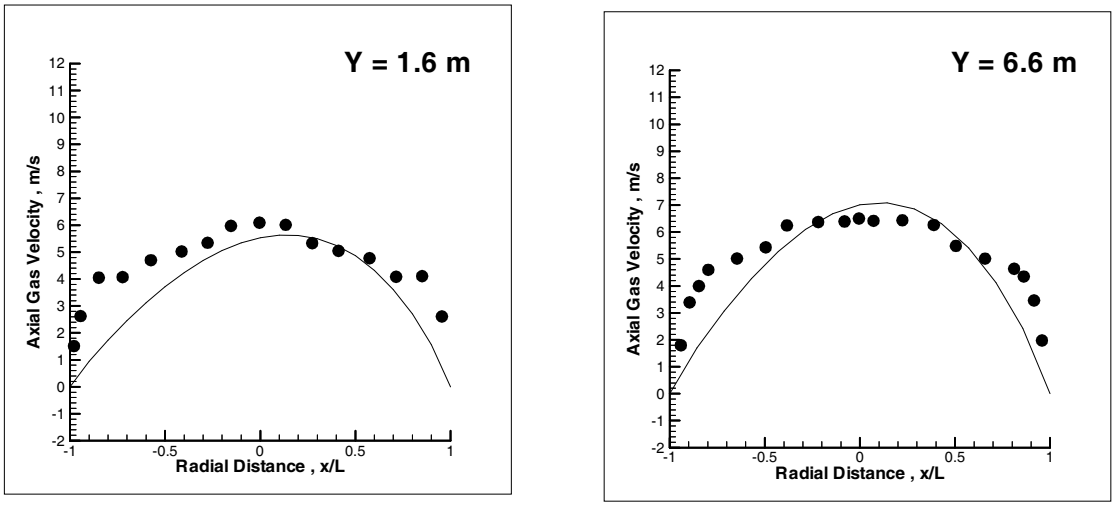

Figure 3. Calculated radial distribution of the axial gas velocity .vs. experimental data [29, 30]

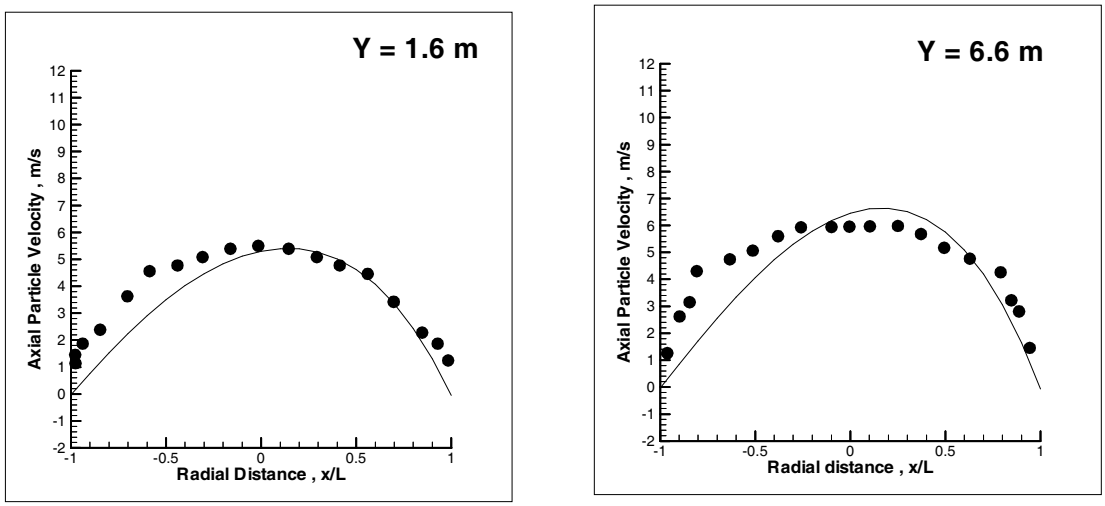

Figure 4. Calculated radial distribution of the axial particle velocity.vs. experimental data [29,30]

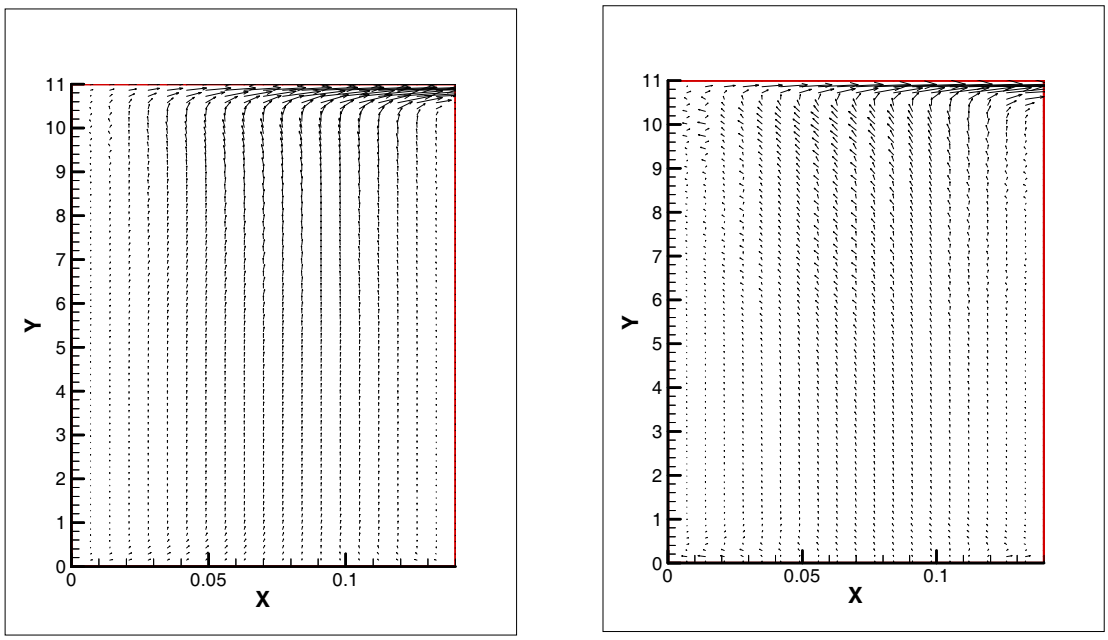

Figure 5. Predicted flow fields of the gas and particle phases in the riser section of the fluidized bed reactor

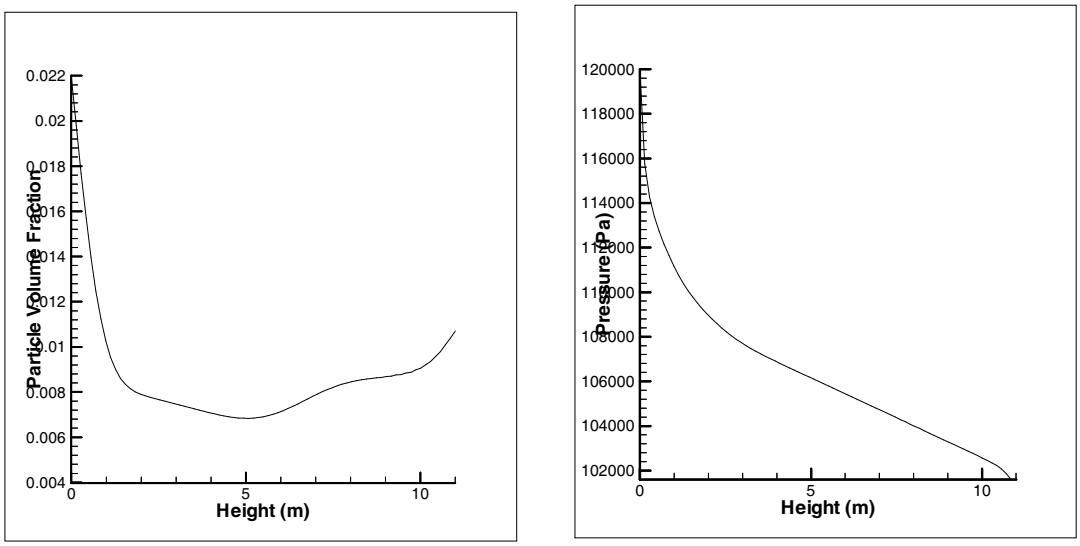

Figure 6. Time-averaged axial particle volume fraction and pressure distribution in the riser section of the fluidized bed reactor

References

1. Xu B.M. and A.B. Yu, "Numerical Simulation of the Gas-Solid Flow in a Fluidized Bed by Combining Discrete Particle Method with Computational Fluid Dynamics", Chem. Eng. Sci., 52, S785 (1997).
2. Davidson J.R. and D. Harrison, Fluidized Particles, Cambridge University Press. (1963).
3. Richner D.W., et al., "Computer Simulation of Isothermal Fluidization in Large–scale Laboratory Rigs", AICHE J., 36, 361, (1990).
4. Kunni D. and O. Levenspiel, Fluidization Engineering, Wiley, New York (1969).
5. Fitzgerald T.J. and L.R. Glicksman, "Testing of Cold Scaled Bed modeling for Fluidized Bed Combustors", 7th AICHE Ann. Meet., Washington DC (1983).
6. Glicksman l. R., "Scaling relationships for Fluidized Beds", Chem. Eng. Sci., 39, 1373(1984).
7. Glicksman l.R., "Scaling Relationships for Fluidized Beds", Chem. Eng. Sci., 43, 1419(1988).
8. Blake T.R. and P.J. Chen, "Computer Modeling of Fluidized Bed Coal classification Reactors", Am. Chem. Soc. Symp. Ser., 168, 8(1981).
9. Gidaspow D. and B. Ettehadieh, "Computer Modeling of Sand in a Two-dimensional Bed with a Jet", paper 63a , AICHE Ann. Meet., New Orleans (1981).
10. Gidaspow D., "Hydrodynamics of fluidization and Heat Transfer Supercomputer Applications", Appl. Mech. Res., 39, 1(1986).
11. Gidaspow, D., 1994. Multiphase Flow and Fluidization: Continuum and Kinetic Theory Description. Academic Press.
12. Anderson T.B. and R. Jackson, "Fluid Mechanical Description of Fluidized Beds, Equations of Motion", Ind. Eng. Chem. Fund. , 6, 527 (1967).
13. Pritchett J.W., T.R. Blake and S.K. Garg, "A Numerical Model of GAS Fluidized Beds," AICHE Symp. Ser., 74(176), 134 (1978).
14. Jackson, R., "Hydrodynamic Stability of Fluid-Particle Systems", Fluidization, J.F. Davidson, R. Clift, D. Harrison, eds., Academic Press, 47(1985).
15. Kuipers J.A.M. and et al., "A Numerical Model of Gas-Fluidized Beds", chem. Eng. Sci., 47, 1913(1992).
16. Kuipers J.A.M. and et al., "Computer Simulation of the hydrodynamics of a Two-Dimensional Gas-Fluidized Beds", Comput. Chem. Eng., 17, 839 (1993).
17. Alves J.J.N. and M. Mori, "Fluid Dynamic Modeling and Simulation of Circulating Fluidized Bed Reactors Analysis of Particle Phase Stress Models", Comput. Chem. Eng., 22, S763 (1998).
18. Wen Y.C. and Y.H. Yu, 1966, Chem. Eng. Prog. Symp. Ser., 62(62), 100.
19. Gidaspow D. and B. Ettehadieh, "Fluidization in Two-Dimensional Beds with a Jet. II: Hydrodynamic Modeling", Ind. Eng. Chem. Fundam., 22, 193(1983).
20. Bird R.B., Stewart W.E., Lightfoot E.N., 1960, Transport Phenomena, Wiley, New York.
21. Massoudi M., Rajagopal K.R. and et al., "Remarks on the Modeling of Fluidized Systems", AICHE J., 38, 471 (1992).
22. Ding J. and D. Gidaspow, "A Bubbling Fluidization Model Using Kinetic Theory of Granular flow", AICHE J., 36, 523(1990).
23. Famili M.H.N, M. K. Moraveji, "A New Finite Volume Based Finite Element Method for Solving the Incompressible Viscous Flow for high Reynolds Number", submitted to Scientia Iranica, 2003.
24. Rhie, C.M., and Chow, W.L., "Numerical Study of the Turbulent Flow Past an Airfoil with Trailing Edge", AIAA Journal, Vol. 21, No.11, pp. 1525-1532 (1983).
25. Schneider, G.E., Raw, M.J., "Control-Volume Finite Element Method for Heat Transfer and Fluid Flow Using Co-located Variables –1. Computational Procedure", Numerical Heat Transfer, Vol. 11, pp. 363-391(1987).
26. Schneider, G.E., Raw, M.J., "A New Control-Volume Finite Element Method Procedure For Heat Transfer and Fluid Flow Using Co-located Variables –2. Application and Validation", Numerical Heat Transfer, Vol. 11, pp. 391-400 (1987).
27. Karimian, S.M.H., and Schneider, G. E.,

"Pressure Based Computational Method for Compressible and Incompressible Flows", Journal of Thermophysics and Heat Transfer, Vol. 8, No. 2, 1994, pp. 267-274.

28. Schneider, G.E, "Advances in Control Volume Based Finite Element Method for Compressible Flows", Second North American Soviet Workshop on Computational Aerodynamics, Montreal Canada, Sep. 3-5, 1991.
29. Yang, Y.L., "Experimental and theoretical studies on hydrodynamics in concurrent upward and downward circulating fluidized beds", PhD Diss., Tsinghua university, Beijing, China (1991).
30. Gao, J., C. Xu, S. Liin and G. Yang, "Advanced model for turbulent gas-solid flow and reaction in FCC riser reactors", AICHE J., Vol. 45, No. 5, Pp 1095-1113 (1999).
31. Launder, B.E., and D.B. Spalding, Mathematical Models of Turbulence, Academic Press, London (1972)